IOP Publishing Journal of Physics: Condensed Matter
J. Phys.: Condens. Matter **32** (2020) 235901 (7pp) https://doi.org/10.1088/1361-648X/ab76e2

# Pressure-induced superconductivity in $SnSb_2Te_4$

**Peng Song[1,2], Ryo Matsumoto[1,2], Zhufeng Hou[3], Shintaro Adachi[1], Hiroshi Hara[1,2], Yoshito Saito[1,2], P B Castro[1,2], Hiroyuki Takeya[1] and Yoshihiko Takano[1,2]**

[1] International Center for Materials Nanoarchitectonics (MANA), National Institute for Materials Science, 1-2-1 Sengen, Tsukuba, Ibaraki 305-0047, Japan
[2] University of Tsukuba, 1-1-1 Tennodai, Tsukuba, Ibaraki 305-8577, Japan
[3] State Key Laboratory of Structural Chemistry, Fujian Institute of Research on the Structure of Matter (FJIRSM), Chinese Academy of Sciences, Fuzhou, 350002 Fujian, People's Republic of China

E-mail: SONG.Peng@nims.go.jp

Received 23 August 2019, revised 20 January 2020
Accepted for publication 17 February 2020
Published 12 March 2020

**Abstract**

Here we firstly report the pressure-induced superconductivity in phase change materials $SnSb_2Te_4$. Single crystals of $SnSb_2Te_4$ were grown using a conventional melting-down method. The resistance under pressure was measured using an originally designed diamond anvil cell with boron-doped diamond electrodes. The temperature dependence of the resistance under different pressures has been measured up to 32.6 GPa. The superconducting transition of $SnSb_2Te_4$ appeared at 2.1 K ($T_c^{onset}$) under 8.1 GPa, which was further increased with applied pressure to a maximum onset transition temperature 7.4 K under 32.6 GPa.

Keywords: superconductivity, data-driven science, phase change material

(Some figures may appear in colour only in the online journal)

## 1. Introduction

Phase change materials (PCMs) are distinguished by their excellent optical and electrical properties and the fast switching between amorphous and crystalline phase and thus are widely used in optics and data storage [1, 2]. Most PCMs are composed of group IV–VI elements, such as $GeSb_2Te_4$ and $GeSb_2Te_5$, and the Fermi level of these compounds at ground states is often located inside the band gap, exhibiting semiconducting properties [3]. Recently, superconducting properties of these binary or ternary PCMs, such as SnTe [4], $Sb_2Te_3$ [5], $GeSb_2Te_4$ [6] have been found whenever pressure is applied or carriers are introduced. First-principles calculations have shown that the high-pressure phase ($Pm\bar{3}m$) of SnTe is metallic and has a very flat band near the Fermi level [7], which is favorable to the formation of the cooper pairs [8]. At high pressure, SnTe can transform into body-center-cubic (BCC) structure with a superconducting critical temperature of ~7.5 K [9], which is in accord with the theoretically predicted value of 7.16 K [7]. The superconductivity in $Sb_2Te_3$ indicates that the crystal structure of the compound remains stable at lower pressure and a Dirac cone remains stable at pressure of 6.9 GPa [5, 10]. These results provide strong support the occurrence of superconductivity in the lower pressure range of the ambient phase is topological related [10]. $GeSb_2Te_4$ (GST) can not only undergo phase transition from an amorphous phase (a-GST) to a crystalline (c-GST) by elevated temperatures [11, 12], but also can have a metal-to-insulator transition at elevated pressure [13]. This transition can be explained as a disorder-induced Anderson localization [14]. Recently,pressure-induced superconductivity transition has been reported in GST and shows that this compound undergo a phase transition from an amorphous GST to bcc GST (b-GST) [6, 15]. One interesting point is that superconducting transition disappears at 43.3 GPa at the phase of b-GST, strongly suggesting a second-order quantum phase transition (QPT) [6]. Thus, the high pressure is an effective approach to study the structural properties in this type of compounds without introducing disorders or impurities. The application of pressure has been reported to turn the $A_2B_3$-type topological insulator $Sb_2Te_3$ [5], $Bi_2Se_3$ [16], and $Bi_2Te_3$ [17] into superconducting state.

 

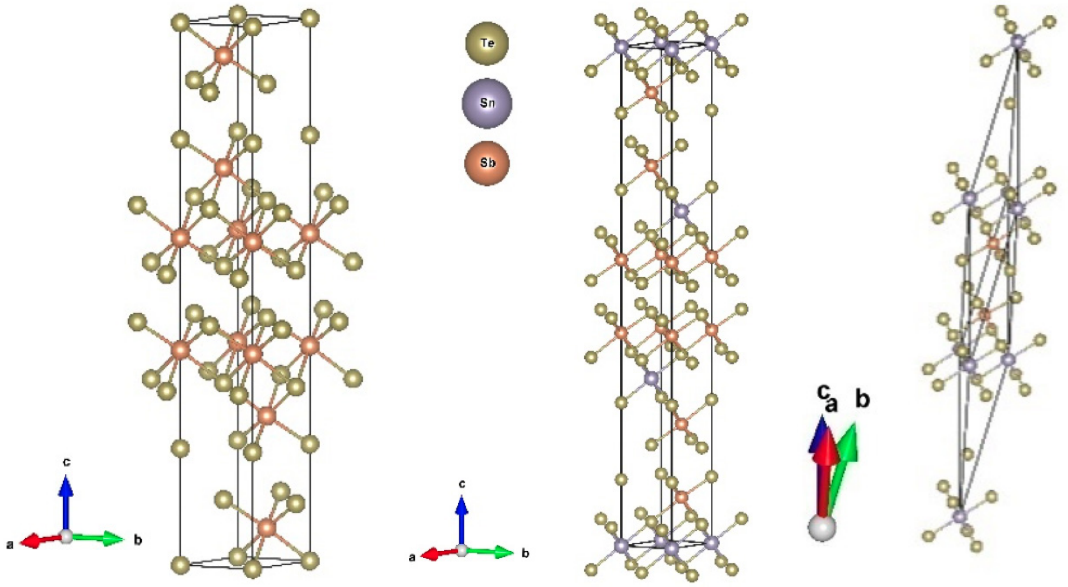


(a) (b) (c)

**Figure 1.** Crystal structures of (a) parent compound of $Sb_2Te_3$ and (b) $SnSb_2Te_4$. (c) Primitive cell of $SnSb_2Te_4$. The figures were drawn using VESTA [32]. Brown, green yellow, and gray balls represents for Sb, Te, and Sn atoms, respectively.

Here we focus on the PCM $SnSb_2Te_4$, which can be considered as a mixture of SnTe and $Sb_2Te_3$, with a similar temperature-dependent phase transition to GST [11, 12, 18] as it can be considered a mixture of SnTe and $Sb_2Te_3$. The analysis of both bulk and surface electronic structure indicates that these compounds are also topological related [19] and have a large penetration depth of the topological surface state (TSS) [20]. It is of great interest to check whether this ternary compound would exhibit superconductivity under applied pressure. Herein we studied the pressure-dependent structure and electronic properties on both theoretical and experimental in $SnSb_2Te_4$.

## 2. Method

The structure properties and electronic structure of $SnSb_2Te_4$ were calculated using the projector augmented wave (PAW) method, as implemented in the Quantum ESPRESSO software package [21, 22]. The generalized gradient approximation (GGA) of Perdew–Burke–Erzerhof (PBE) [23] was used to describe the exchange-correlation function. The inner 4d-electrons in Sn and Sb are treated as valence electrons. A $10 \times 10 \times 10$ $k$-grid was employed for the $k$-point sampling in the first Brillouin zone and the kinetic energy cutoffs for the expansion of electronic wave function was set to 74 Ry. The atomic positions and lattice parameters were relaxed using the Broyden–Fletcher–Goldfard–Shanno (BFGS) algorithm. In the density of states (DOS), a $k$-mesh size of $20 \times 20 \times 20$ was used. The crystal orbital Hamiltonian population (COHP) [24] and its energy integral (ICOHP) were used for the analysis of chemical bonding, implemented in LOBSTER tool [25].

Single crystals of $SnSb_2Te_4$ were grown using a conventional melting method. Sn (99.9%, powder), Sb (99.99%, powder), Te (99.9%, grain), combined in stoichiometric ratios in an evacuated silica tube. Afterward, the tube was put into a furnace and heated up to 1010 K for 10 h. The samples were then slowly cooled to 873 K at a rate of 9.1 K $h^{-1}$ and held for 24 h. Powder x-ray diffraction was conducted by mini flex 600 (Rigaku) with Cu K$\alpha$ (=1.5406 Å) radiation. The compositional ratios were investigated by energy-dispersive spectrometry (EDX) using a JSM-6010LA (JEOL). The temperature dependence of resistance under high pressure was measured by boron-doped diamond anvil cells (DAC) [26], implemented in a physical property measurement system (quantum design PPMS). The electrodes at the bottom anvil were fabricated by boron-doped diamond synthesized using a microwave plasma-assisted chemical vapor deposition (MPCVD) technique [27] and were separated by an insulating undoped diamond (UDD) layer. The fabrication process details of this bottom anvil cell are described in [26, 28]. The gasket was a stainless steel with a thickness of 200 $\mu$m. Cubic boron nitride (cBN) powder with ruby manometer was used as a pressure-transmitting medium. The ruby powder was mixed in cBN and was used to measure the applied pressure by the fluorescence from ruby [29] and the Raman spectrum from the culet of top diamond anvil by an inVia Raman microscope (RENISHAW).

## 3. Results and discussion

Figure 1 shows the crystal structures of $SnSb_2Te_4$ and its parent compound $Sb_2Te_3$. $SnSb_2Te_4$ has a trigonal structure with space group $R\bar{3}M$ (lattice constants of $a = b = 4.3158$ Å and $c = 41.6574$ Å) at ambient pressure [19, 30]. The intermediate layers of $Sb_2Te_3$ and $SnSb_2Te_4$ are almost identical, and each Sb atom is coordinated with four Te atoms. The structure difference between $SnSb_2Te_4$ and $Sb_2Te_3$ is that

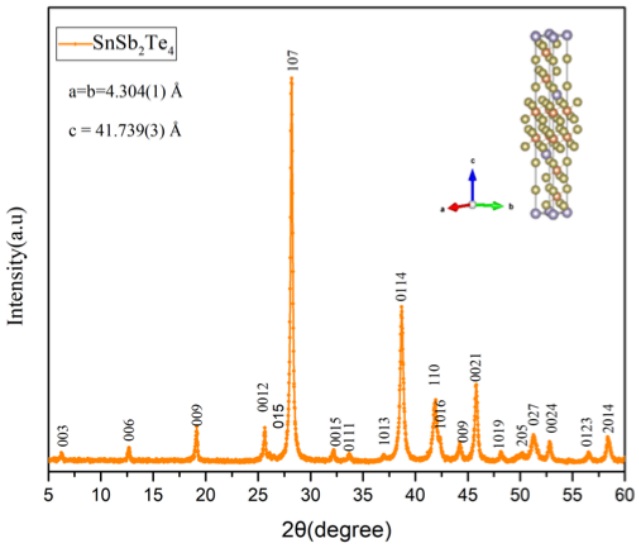


**Figure 2.** Room temperature x-ray diffraction patterns of $SnSb_2Te_4$.

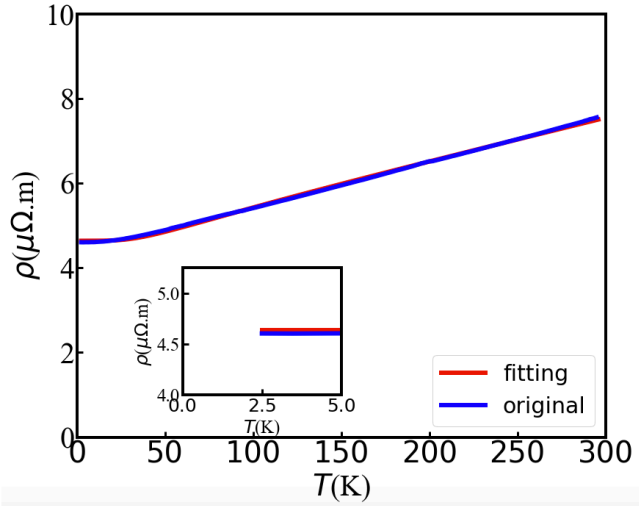


**Figure 3.** Temperature dependent resistivity of $SnSb_2Te_4$.

the central Te2 layer in $Sb_2Te_3$ is replaced by the Te2–Sn–Te2 layer in $SnSb_2Te_4$. This ternary compound is weakly bonded by van der Waals interaction between Te layers [12, 31]. By a certain heat treatment, the $SnSb_2Te_4$ also transform into a NaCl-type FCC structure [18]. Figure 2 shows the powder XRD pattern of $SnSb_2Te_4$. The peaks were corresponding to a $R\bar{3}M(H)$ structure of $SnSb_2Te_4$, with a lattice constant of $a = b = 4.304(1)$ Å and $c = 41.739(3)$ Å. Sn Sb and Te are very uniformly distributed in this material. Using EDS to analyze its composition, the ratio of the material was shown as $Sn_{1.01}Sb_{1.98}Te_4$, which shows good agreements with nominal composition.

The temperature dependence of the resistivity for $SnSb_2Te_4$ are shown in figure 3, measured from 2.5 K to 296 K. The resistivity of $SnSb_2Te_4$ decreases with decreasing temperature which is in good agreement with metallic behavior. In non-magnetic metals, the temperature dependence of resistivity is mainly derived from electron–phonon interactions and can be expressed by Bloch–Gruneissen formula [32].

$$\rho(T) = \rho(0) + \alpha_{\mathrm{el-ph}}\left(\frac{T}{\Theta_R}\right)^5 \int_0^{\frac{\Theta_R}{T}} \frac{x^5}{(\mathrm{e}^x - 1)(1 - \mathrm{e}^{-x})}\mathrm{d}x, \quad (1)$$

where $\rho(0)$ is the residual resistivity due to defect scattering and is independent of temperature, $\Theta_R$ is the Debye temperature, and $\alpha_{\mathrm{el-ph}}$ is a constant associated with the electron–phonon coupling constant $\lambda$. The red line of figure 3 is the fitted equation from 2.5 K to 296 K and the Debye temperature can be obtained close to 353 K, which is much larger the $Sb_2Te_3$($\Theta_R = 200$ K) [33] and SnTe ($\Theta_R = 165$ K) [34]. It is known from the BCS theory that the Debye temperature is positively correlated to the critical temperature $T_c$ [35]. Therefore, This will also convince us that $SnSb_2Te_4$ can exhibit superconducting properties under pressurized conditions.

Figure 4 shows the calculated band structure, DOS, and COHP of $SnSb_2Te_4$ at ambient pressure. We also present the band structure of $SnSb_2Te_4$ (figure 4(d)) under high pressure of 10 GPa for a comparison. We can see that this compound is a semiconductor with a narrow band-gap (0.26 eV obtained by the present GGA-PBE calculations) at the Z point. The energy bands near the top of valence bands and the bottom of conduction bands are both flat, and thus the valence and conduction band edges have high DOS. The orbital-decomposed DOS reveals that the conduction band of $SnSb_2Te_4$ is mainly composed of Sn-5p, Sb-5p and Te-5p states, and there is also an additional contribution from Te-5s states. The valence bands from −5 eV to −1 eV are mainly contributed by the hybridization between the Sn-(and Sb-) 5p and Te-5p orbitals, while the bands from −1 eV to the valence band maximum (VBM) are contributed by the hybridization between the Sn-(and Sb-) 5s states between the Te 5p orbitals. Figure 4(c) shows the calculated—pCOHP for the nearest-neighboring atom pairs of Sn–Te and Sb–Te, in which the positive (negative) of—pCOHP values correspond to the bonding (anti-bonding) characteristics. Therefore, we can see that the Sn-5p (and Sb-5p) and Te-5p orbitals form the bonding states in the energy range from −5 eV to −1 eV, while the Sn-5s (Sb-5s) and Te-5p orbitals form the anti-bonding states in the energy range from −1 eV to the VBM. The anti-bonding states, which come from the hybridization between the Sn-5p (Sb-5p) and Te-5p, appear in the vicinity of conduction band bottom (CBM).

Compared with the Sb–Te bond length in $Sb_2Te_3$, the Sn–Te and Sb–Te bond lengths in $SnSb_2Te_4$ have negligible change (0.02 Å at most). The characteristics of chemical bonding between Sb–Te in two compounds are very similar. It is noted that the energy levels of Sn 5s (5p) are shallower than those of Sb. Therefore, $SnSb_2Te_4$ has a smaller energy gap than $Sb_2Te_3$. Figure 4(d) shows the band structure of $SnSb_2Te_4$ under pressure of 10 GPa. It can be seen that the Fermi level crosses the top valence bands, indicating the pressure-induced a decrease of the band gap of $SnSb_2Te_4$ and a transition to metallic behavior. As mentioned above, the anti-bonding characteristic appears both in the vicinity of VBM and CBM of $SnSb_2Te_4$. If the crystal structure does not transform into a different phase under high pressure, the applied pressure will usually lead to a decrease of bond lengths between atoms. For $SnSb_2Te_4$, the

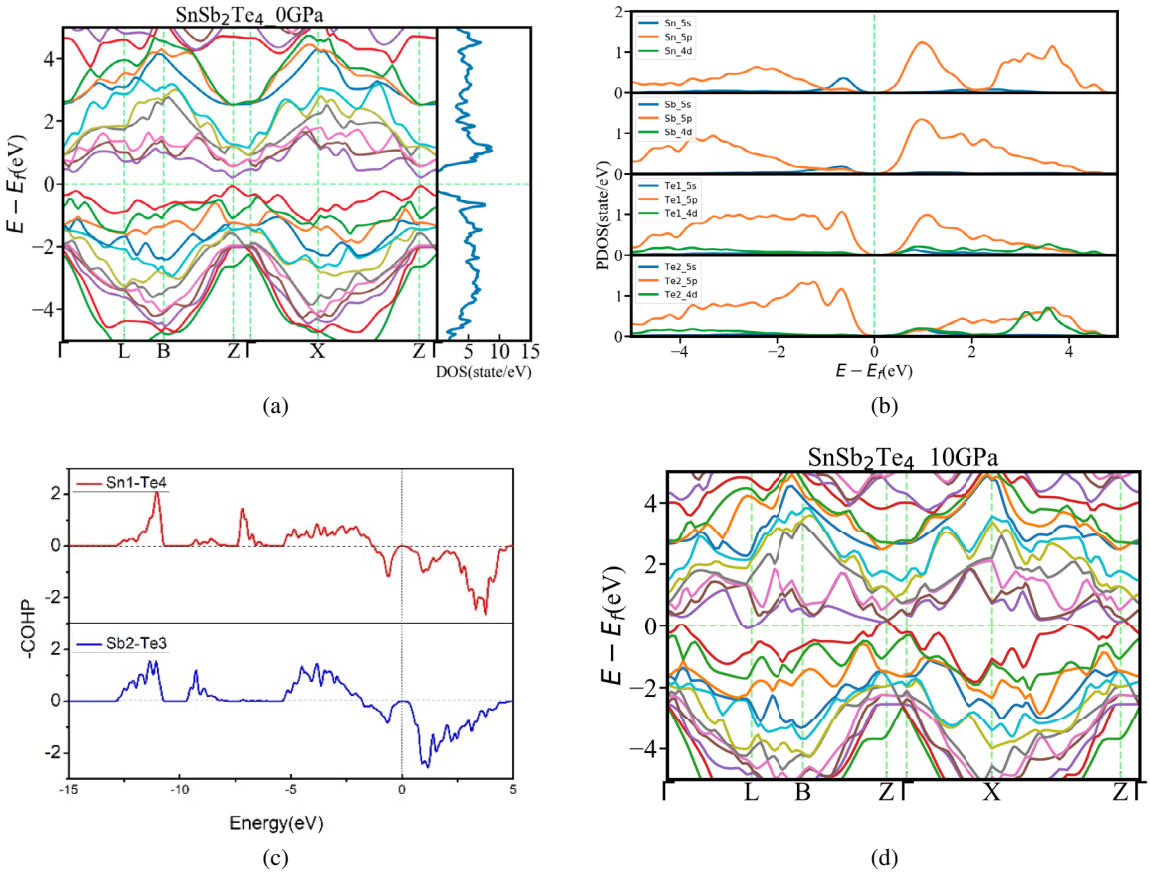


**Figure 4.** (a) Band structure of $SnSb_2Te_4$ and electron DOS of $SnSb_2Te_4$ (b) projected density of state (PDOS) (c) the calculated crystal orbital Hamilton population for the $SnSb_2Te_4$ at zero pressure (d) the comparative band structure at 10 GPa.

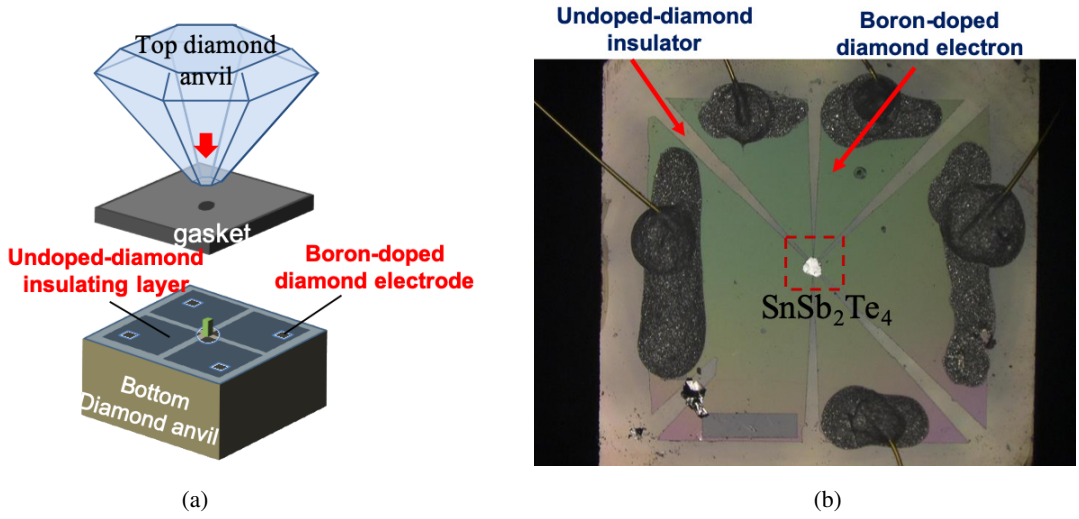


**Figure 5.** (a) Boron-doped diamond anvil cell, (b) the image of sample in the bottom diamond anvil.

applied pressure results in the shrinking of Sn–Te and Sb–Te bond lengths and thus the anti-bonding states near the VBM and CBM would both shift toward high energy. This might be the reason why the band gap of $SnSb_2Te_4$ decreases as the applied high pressure. The similar trend was also found in our previous studies for $SnBi_2Se_4$ [36], $PbBi_2Te_4$ [37], and $AgIn_5Se_8$ [37].

Figure 5 shows measurement system of temperature-dependence of resistance using the originally designed diamond-anvil cell [26]. The sample voltage is detected by heavily boron-doped metallic diamond (BDD) electrodes on the bottom anvil. In measurement of $SnSb_2Te_4$, a five-probe design of electrodes was used as shown in figure 5(a). Figure 5(b) shows an image of the sample space of our DAC. The sample was placed at the center of the bottom anvil and measured by a standard four-probe method. Prior to applying pressure, the crystal was cleaved with a scotch tape in order to remove the oxidized surface.

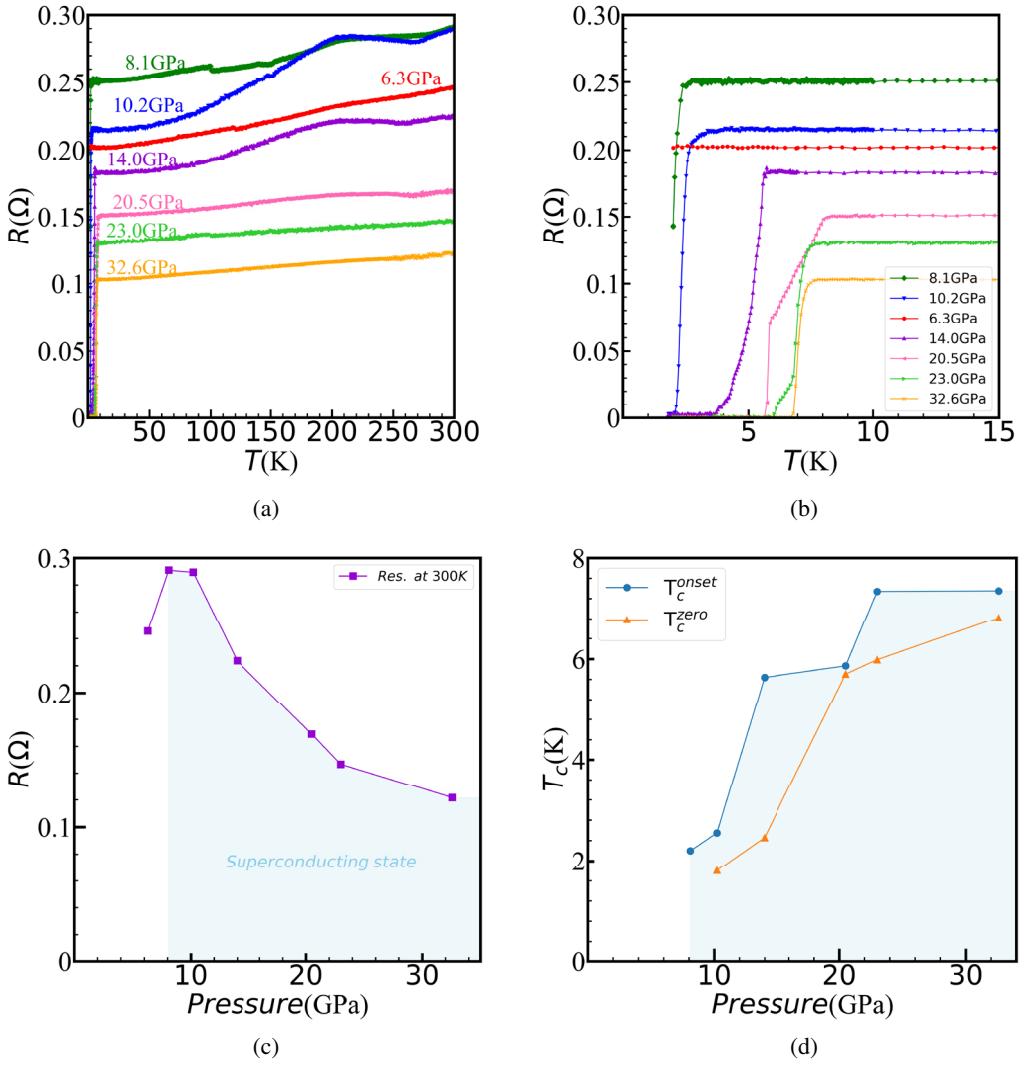


**Figure 6.** (a) temperature dependence of resistance from 2 K to 300 K (b) temperature dependence of resistance from 2 K to 15 K (c) pressure dependence of resistance from 6.3 GPa to 32.6 GPa (d) superconducting phase diagram.

Figure 6(a) shows the transport measurements at low temperature at pressures between 6.3 GPa to 32.6 GPa. Under these pressures, the measured temperature-dependent resistance of $SnSb_2Te_4$ reveals a significant metallic behavior for the temperature above 10 K. It is also apparent that superconductivity begins to occur at 8.1 GPa with $T_c^{onset} \sim 2$ K and the zero resistivity was observed at 10.2 GPa with $T_c^{zero} \sim 2.2$ K. At a further increase of pressure, in the range between 10.2 and 23 GPa, the superconducting transition temperature increases with increasing pressure. Figure 6(c) shows pressure-dependent electrical resistance at 300 K. From 6.3 GPa to 10.2 GPa, the resistance appears to rise first and then decrease. From our band structures of $SnSb_2Te_4$ under high pressure, we found that the applied pressued at 10 GPa lead to the closing of band gap of $SnSb_2Te_4$, i.e. a semiconductor-to-metal transition. At 10.2 GPa, a resistance kink was observed in the *R–T* curve. The same phenomenon also occurs in charge-density-wave (CDW) materials such as $VSe_2$ [38] and $NbTe_4$ [39]. In $NbTe_4$, CDW is gradually suppressed to disappear as pressure increases and superconductivity emerges. In $VSe_2$, CDW increases with increasing pressure. Above 12 GPa, CDW state is suppressed, and superconducting phase begins to appear at 15.2 GPa. These two materials have certain similarities in the crystal structure with $SnSb_2Te_4$. Such a kink in the pressure-dependent *R*(300 K) around 10–12 GPa may be due to the pressure-induced phase transition.

Figure 6(d) shows the superconducting phase diagram of the $SnSb_2Te_4$ single crystal. From 14.0 GPa to 23.0 GPa, there are some differences between the $T_c^{zero}$ and $T_c^{onset}$ values. It can be seen from figure 6(b) that there are two superconducting transition temperatures at these points, which are likely to have structure phase transition in these pressure range. As the pressure increased, this compound was transferred into a more stable structure phase, resulting in a unique sharp superconductor transition. In the parent compound $Sb_2Te_3$, from 22.3 GPa to 26.9 GPa, some *R–T* curves similar to $SnSb_2Te_4$ were also observed. And it can be seen from its phase diagram that there are multiple phases of $Sb_2Te_3$ under these pressures [5]. Similarly, the same phenomenon was observed in the $GeSb_2Te_4$ [6]. Therefore, in $SnSb_2Te_4$, there are likely to be multiple phases from 14.0 GPa. According the context of Bardeen–Cooper–Schrieffer (BCS) superconductivity

theory [40], $\kappa T_c = \hbar\omega_{ph} e^{-1/\lambda N(E_F)}$, where $\kappa$ is the Boltzmann constant, $\hbar\omega_{ph}$ is a phonon energy, $\lambda$ is the electron–phonon coupling constant, and $N(E_F)$ is the DOS at the Fermi level. Therefore, increasing the DOSs at the Fermi level contributes to the transition from a normal conductor to a superconductor. We have found that in the cases of semiconductor compounds at ambient pressure with anti-bonding states near valence and conduction band edges, the energy gap tends to decrease with increasing pressure when the applied pressure is not large. Based on our previous work [36, 37], the compounds with flat band near the Fermi level and an anti-bonding state in bonding region were very likely to show the pressure-induced superconductivity. Pressure-induced superconductivity in $SnSb_2Te_4$ provided a strong support to this hint.

## 4. Conclusion

We studied the band structure information of $SnSb_2Te_4$ via first-principles calculation. We found that $SnSb_2Te_4$ had anti-bonding state at the valence and conduction band edges. It should be noticed that many pressure-induced superconductors in our previous papers share similar characteristics. The $SnSb_2Te_4$ undergoes a superconducting transition with $T_c^{onset} \sim 2$ K when a pressure of 8.1 GPa is applied. With further increase of pressure, the systems reach a maximum of $T_c^{onset} \sim 7.4$ K, around 32.6 GPa. With increase of the pressure up to 32.6 GPa, $T_c$ enhances continuously without saturation. Based on the existing *R–T* data, we have also made some discussions to provide some reference for future researchers.

## Acknowledgments

P Song would like to thank Mr Yan Meng for a further discussion about manuscript. This work was partly supported by JST CREST Grant No. JPMJCR16Q6, JST-Mirai Program Grant No. JPMJMI17A2, JSPS KAKENHI Grant No. JP17J05926, 19H02177, and the 'Materials research by Information Integration' Initiative ($MI^2I$) project of the Support Program for Starting Up Innovation Hub from JST. The computation in this study was performed on Numerical Materials Simulator at NIMS.

## ORCID iDs

Peng Song https://orcid.org/0000-0002-9918-2734
Zhufeng Hou https://orcid.org/0000-0002-0069-5573

## References

[1] Wuttig M and Yamada N 2007 Phase-change materials for rewriteable data storage *Nat. Mater.* **6** 824–32
[2] Raoux S, Wejcnic W and Ielmini D 2010 Phase change materials and their application to nonvolatile memories *Chem. Rev.* **110** 240–67
[3] Matsunaga T, Kojima R, Yamada N, Kifune K, Kubota Y, Tabata Y and Takata M 2006 Single structure widely distributed in a GeTe–$Sb_2Te_3$ pseudobinary system: a rock salt structure is retained by intrinsically containing an enormous number of vacancies within its crystal *Inorg. Chem.* **45** 2235–41
[4] Timofeev Y A, Vinogradov B V, Yakovlev E N, Kapitanov E V and Kuzyan R O 1982 Superconductivity of stannous telluride at high pressure *Sov. Phys.—Solid State* **24** 1780–1
[5] Zhao J, Liu H, Ehm L, Chen Z, Sinogeikin S, Zhao Y and Gu G 2011 Pressure-induced disordered substitution alloy in $Sb_2Te_3$ *Inorg. Chem.* **50** 11291–3
[6] Hen B, Layek S, Goldstein M, Shelukhin V, Shulman M, Karpovski M, Greenberg E, Sterer E, Dagan Y, Rozenberg G K and Palevski A 2018 Superconductor-insulator transition in fcc $GeSb_2Te_4$ at elevated pressures *Phys. Rev.* B **97** 024513
[7] Zhou D, Li Q, Ma Y, Cui Q and Chen C 2013 Pressure-induced superconductivity in SnTe: a first-principles study *J. Phys. Chem.* C **117** 12266–71
[8] Deng S, Simon A and Köhler J 2005 A 'flat/steep band' model for superconductivity *Int. J. Mod. Phys.* B **19** 29–36
[9] Timofeev Y A, Vinogradov B V, Yakovlev E N, Kapitanov E V and Kuzyan R O 1982 Superconductivity of tin tellurides at high pressure *Fiz. Tverd. Tela* **24** 3143–4
[10] Zhu J *et al* 2013 Superconductivity in topological insulator $Sb_2Te_3$ induced by pressure *Sci. Rep.* **3** 2016
[11] Zhang W, Thiess A, Zalden P, Zeller R, Dederichs P H, Raty J-Y, Wuttig M, Blügel S and Mazzarello R 2012 Role of vacancies in metal-insulator transitions of crystalline phase-change materials *Nat. Mater.* **11** 952
[12] Da Silva J L F, Walsh A and Lee H 2008 Insights into the structure of the stable and metastable $(GeTe)_m(Sb_2Te_3)_n$ compounds *Phys. Rev.* B **78** 224111
[13] Xu M, Cheng Y Q, Wang L, Sheng H W, Meng Y, Yang W G, Han X D and Ma E 2012 Pressure tunes electrical resistivity by four orders of magnitude in amorphous $Ge_2Sb_2Te_5$ phase-change memory alloy *Proc. Natl Acad. Sci.* **109** E1055–62
[14] Siegrist T, Jost P, Volker H, Woda M, Merkelbach P, Schlockermann C and Wuttig M 2011 Disorder-induced localization in crystalline phase-change materials *Nat. Mater.* **10** 202–8
[15] Greenberg E *et al* 2017 Superconductivity in multiple phases of compressed $GeSb_2Te_4$ *Phys. Rev.* B **95** 064514
[16] Hamlin J J, Jeffries J R, Butch N P, Syers P, Zocco D A, Weir S T, Vohra Y K, Paglione J and Maple M B 2011 High pressure transport properties of the topological insulator $Bi_2Se_3$ *J. Phys.: Condens. Matter* **24** 035602
[17] Zhang J L *et al* 2010 Pressure-induced superconductivity in topological parent compound $Bi_2Te_3$ *Proc. Natl Acad. Sci.* **108** 24–8
[18] Schäfer T, Konze P M, Huyeng J D, Deringer V L, Lesieur T, Müller P, Morgenstern M, Dronskowski R and Wuttig M 2017 Chemical tuning of carrier type and concentration in a homologous series of crystalline chalcogenides *Chem. Mater.* **29** 6749–57
[19] Menshchikova T, Eremeev S and Chulkov E 2013 Electronic structure of $SnSb_2Te_4$ and $PbSb_2Te_4$ topological insulators *Appl. Surf. Sci.* **267** 1–3
[20] Niesner D *et al* 2014 Bulk and surface electron dynamics in a *p*-type topological insulator $SnSb_2Te_4$ *Phys. Rev.* B **89** 081404
[21] Giannozzi P *et al* 2009 Quantum ESPRESSO: a modular and open-source software project for quantum simulations of materials *J. Phys.: Condens. Matter* **21** 395502
[22] Giannozzi P *et al* 2017 Advanced capabilities for materials modelling with quantum ESPRESSO *J. Phys.: Condens. Matter* **29** 465901
[23] Perdew J P, Chevary J A, Vosko S H, Jackson K A, Pederson M R, Singh D J and Fiolhais C 1992 Atoms, molecules, solids, and surfaces: applications of the

generalized gradient approximation for exchange and correlation *Phys. Rev.* B **46** 6671–87
[24] Dronskowski R and Bloechl P E 1993 Crystal orbital Hamilton populations (COHP): energy-resolved visualization of chemical bonding in solids based on density-functional calculations *J. Phys. Chem.* **97** 8617–24
[25] Maintz S, Deringer V L, Tchougréeff A L and Dronskowski R 2016 LOBSTER: a tool to extract chemical bonding from plane-wave based DFT *J. Comput. Chem.* **37** 1030–5
[26] Matsumoto R, Sasama Y, Fujioka M, Irifune T, Tanaka M, Yamaguchi T, Takeya H and Takano Y 2016 Note: novel diamond anvil cell for electrical measurements using boron-doped metallic diamond electrodes *Rev. Sci. Instrum.* **87** 076103
[27] Takano Y, Nagao M, Takenouchi T, Umezawa H, Sakaguchi I, Tachiki M and Kawarada H 2005 Superconductivity in polycrystalline diamond thin films *Diam. Relat. Mater.* **14** 1936–8
[28] Matsumoto R, Yamashita A, Hara H, Irifune T, Adachi S, Takeya H and Takano Y 2018 Diamond anvil cells using boron-doped diamond electrodes covered with undoped diamond insulating layer *Appl. Phys. Express* **11** 053101
[29] Barnett J D, Block S and Piermarini G J 1973 An optical fluorescence system for quantitative pressure measurement in the diamond-anvil cell *Rev. Sci. Instrum.* **44** 1–9
[30] Concas G, de Pascale T, Garbato L, Ledda F, Meloni F, Rucci A and Serra M 1992 Electronic and structural properties of the layered $SnSb_2Te_4$ semiconductor: *ab initio* total-energy and Mössbauer spectroscopy study *J. Phys. Chem. Solids* **53** 791–6
[31] Axilrod B M and Teller E 1943 Interaction of the van der Waals type between three atoms *J. Chem. Phys.* **11** 299–300
[32] Goetsch R J, Anand V K, Pandey A and Johnston D C 2012 Structural, thermal, magnetic, and electronic transport properties of the $LaNi_2(Ge_{1-x}P_x)_2$ system *Phys. Rev.* B **85** 054517
[33] Chen X, Zhou H D, Kiswandhi A, Miotkowski I, Chen Y P, Sharma P A, Lima Sharma A L, Hekmaty M A, Smirnov D and Jiang Z 2011 Thermal expansion coefficients of $Bi_2Se_3$ and $Sb_2Te_3$ crystals from 10 K to 270 K *Appl. Phys. Lett.* **99** 261912
[34] Bauer Pereira P, Sergueev I, Gorsse S, Dadda J, Müller E and Hermann R P 2013 Lattice dynamics and structure of GeTe, SnTe and PbTe *Phys. Status Solidi* b **250** 1300–7
[35] Ashcroft N W 1968 Metallic hydrogen: a high-temperature superconductor? *Phys. Rev. Lett.* **21** 1748–9
[36] Matsumoto R, Hou Z, Hara H, Adachi S, Takeya H, Irifune T, Terakura K and Takano Y 2018 Two pressure-induced superconducting transitions in $SnBi_2Se_4$ explored by data-driven materials search: new approach to developing novel functional materials including thermoelectric and superconducting materials *Appl. Phys. Express* **11** 093101
[37] Matsumoto R *et al* 2018 Data-driven exploration of new pressure-induced superconductivity in $PbBi_2Te_4$ *Sci. Technol. Adv. Mater.* **19** 909–16
[38] Matsumoto R *et al* 2019 Crystal growth, structural analysis, and pressure-induced superconductivity in a AgIn5Se8 single crystal explored by a data-driven approach *Inorg. Chem.* **59** 325–31
[39] Yang X *et al* 2018 Pressure induced superconductivity bordering a charge-density-wave state in $NbTe_4$ with strong spin–orbit coupling *Sci. Rep.* **8** 6298
[40] Suhl H, Matthias B T and Walker L R 1959 Bardeen–Cooper–Schrieffer theory of superconductivity in the case of overlapping bands *Phys. Rev. Lett.* **3** 552–4